NUMERICAL STUDY OF COOLING PERFORMANCE AUGMENTATION FOR PANEL-TYPE RADIATOR UNDER THE CHIMNEY EFFECT

Wenrong SI[a], Shanshan JIN[a], Yiru SHOU[a], Peng YUAN[b], Yuhang TIAN[c], Jian YANG[c*]

[a] State Grid Shanghai Municipal Electrical Power Company, Shanghai 200122, China

[b] Xi'an MaoRong Power Equipment Co., Ltd, Xi'an 710000, China

[c] MOE Key Laboratory of Thermo-Fluid Science and Engineering, Xi'an Jiaotong University, Xi'an 710049, China

[*] Corresponding author; E-mail: yangjian81@mail.xjtu.edu.cn

In order to augment cooling performance of transformer panel-type radiators under natural convection, the fluid flow and heat transfer for a novel panel-type radiator and its surrounding air are numerically studied in this paper. The novel radiator is equipped with wind deflectors on both lateral sides and a chimney cap on the top. Then the effects of the height and channel number of the chimney cap on the cooling performance of the radiator are simulated. The results show that wind deflectors can form several enclosed air channels with radiator fins. The airflow can be accelerated under the chimney effect generated in these channels, and the cooling capacity of the radiator can be increased by 12.75%. The addition of a chimney cap can further extend the chimney channels and increase its cooling capacity by 15.74%. Furthermore, with the increase of the height and channel number, the total cooling capacity of the panel-type radiator increases first and then decreases. In this study, when the chimney cap has five channels and a height of 700 mm, the novel radiator can obtain the best cooling performance, where its cooling capacity and overall heat transfer coefficient can be increased by 26.54% and 28.21%, respectively, as compared with traditional panel-type radiators, and the temperature difference between the inlet and outlet insulating oil is 7.1 ℃

Keywords: *Transformer panel-type radiator; The chimney effect; Natural convection; Cooling performance augmentation; Numerical simulation*

1. Introduction

Transformers are the key equipment in power systems, which are quite important to the economic transmission, flexible distribution and safe use of electric energy [1]. When transformers are working, due to the existence of resistance and magnetoresistance, they will cause core losses and copper loss [2]. The consumed electric energy will eventually be converted into thermal energy, which will increase the winding's temperature. With the increase of transformer capacity, transformer overheating problem aggravates. If transformers are overheated for a long time, not only the power system transmission loss will increase, the output capacity will be far below the rated capacity, but will also cause performance degradation of insulating material, accelerate aging of insulating material,

and shorten the service life of transformer [3]. Therefore, it is essential to upgrade the current cooling system for the transformer [4].

Currently, most of the transformers in service are oil-immersed transformers and the matching radiators are usually panel-type radiators. The cooling modes of the radiator mainly include oil natural air natural (ONAN), oil natural-air forced (ONAF), oil forced-air natural (OFAN), oil forced-air forced (OFAF) and oil directed-air forced (ODAF). Research on the cooling performance of power transformer radiators under different cooling modes was popular in the past years. Some scholars improve the overall heat dissipation performance of the transformer by changing the structure of the oil side flow channel. For example, Cha et al. [5] numerically investigated the influence of the thermal head effect on improving the heat dissipation characteristics of the panel-type radiator. They found that increasing the height difference between the center of the panel-type radiator and the center of the transformer could significantly increase the flow rate of insulating oil and reduce the size and cost of the radiator. Tălu and Tălu [6] numerically optimized the design of the power transformer radiator and studied the influence of the inclination angle of the upper manifold on the temperature distribution of the insulating oil in the radiator at different ambient temperatures. The results showed that the radiator achieved the best cooling performance when the inclination angle of the upper manifold was about 20°. Kim et al. [7] numerically investigated the effect of oil-side and air-side thermal resistance on the total heat transfer coefficient of a panel-type radiator under OFAN mode. They confirmed that the air-side thermal resistance was about 92%-95% of the total thermal resistance, the oil-side thermal resistance was about 5%-7% of the total thermal resistance, and the thermal resistance of the radiator fin was only 0.02%. In addition, they compared the cooling performance under eight new oil channel structures and found that there was only ±3% difference for outlet oil temperature under different configurations.

On the other hand, to enhance the heat transfer on the air-side of the radiator, Min et al. [8] numerically analyzed the flow and heat transfer performance of rectangular winglet pairs set on the surface of an ONAN panel-type radiator. The results showed that the heat transfer coefficients of the radiator were increased by 23.6%-32.0%. Fdhila et al. [9] simplified the numerical modeling of a panel-type radiator in air using an anisotropic porous media approach and presented the effects of the size and number of fans on the cooling performance of the panel-type radiator. The results showed that the cooling performance of multiple small-sized fans was better than a single large-sized fan for the same airflow. Paramane et al. [10] studied the air cooling system for a 25 MVA power transformer under ONAF mode and showed that horizontal fans had higher cooling efficiency than vertical fans. Subsequently, they conducted an experiment [11] to visualize the airflow on the surface of a panel-type radiator using thin strands of cotton and get the temperature distribution using thermography. Kim et al. [12] numerically evaluated the effect of the relative positions of two cooling fans fixed at the bottom and right surfaces of a panel-type radiator, respectively. The results showed that, when the cooling fans were located at the center of the bottom surface and bottom of the right surface, it could lead to the best cooling performance, because of the positive interaction between the vertical and horizontal airflow induced by fans. Garelli et al. [13] numerically investigated the enhanced heat transfer performance of delta-wing vortex generators in a panel-type radiator under ONAN mode. It was found that the overall heat transfer performance of the radiator could be improved by 12% with optimum vortex generator geometric parameters. Li et al. [14] compared the top-oil temperature and hot-spot temperature of the transformer under forced air-cooling and falling film cooling conditions.

They found that falling film cooling was more effective for higher heat dissipation demand of the transformer.

The existing research for the air-side heat transfer of transformer radiators is mainly focused on the influence of fan arrangement on the cooling performance of the radiator, and less research is performed on the heat transfer enhancement of radiator under AN mode. Natural convection heat dissipation is considered as a stable and reliable heat dissipation method without noise and energy consumption [15]. Kim et al. [7] and Rodriguez et al. [16] pointed out that poor air-side natural convection heat dissipation performance under AN mode is the main reason limiting the cooling performance of the panel-type radiator. Natural convection heat transfer can often be enhanced by increasing the surface area of the radiator fin, but this can also result in bigger sizes and higher costs. Natural convection is a phenomenon of buoyancy-driven flow due to the density differences in the fluid caused by temperature differences and gravity. The lack of sufficient driving force to overcome the viscous frictional resistance during natural convection is the main reason for its poor heat transfer performance [17]. This means that new thermal designs are needed to increase air density difference and then increase the driving force of the airflow. For natural convection, a chimney structure can create a pressure difference between the chimney inlet and the surroundings to promote airflow entrainment and increase air flow rate [15], which is known as the chimney effect. The chimney effect has been widely used in building ventilation and solar power generation [18,19], but it was relatively less applied in heat transfer enhancement. Haaland and Sparrow [20] first showed that the chimney effect could accelerate fluid flow in a vertical channel, and numerically solved the natural convection problem for a vertical channel with both a horizontal line source and a uniformly distributed surface source at the inlet. Auletta et al. [21] experimentally studied the effect of adding an adiabatic chimney extension to a vertical isoflux symmetric heating channel. The average wall Nusselt number of the heating channel increased by 10%-20% for different extension channels. Moon et al. [22] investigated the natural convection heat transfer for a finned plate in a chimney channel used for a reactor cavity cooling system. They found that the height and width of the chimney had an important influence on the generation and strength of the chimney effect. Recently, Abbas et al. [23] studied the flow and heat transfer characteristics of an upward horizontal rectangular heat sink with a plastic chimney on the top using experimental and numerical methods. It was confirmed that the low thermal conductivity chimney could create an effective pressure difference at its edge and center to accelerate airflow. Schwurack et al. [24] utilized the chimney effect to improve the thermal performance of a thermoelectric generator (TEG). The results showed that the output power of the TEG with a cooling chimney channel was increased by 46.2%. Fulpagare et al. [25] optimized the flow path of a fully enclosed cabinet by introducing radiators and baffles to form dual chimneys, which can facilitate airflow circulation inside and outside the cabinet. It can be concluded that the chimney effect could help to create a big temperature gradient in natural convection, which could increase the fluid velocity and ultimately enhance heat transfer.

A panel-type radiator can be regarded as an equipment with sustained heat source during the cooling process, and it has the characteristics of gradually decreasing temperature distribution from top to bottom. Thus, its thermal performance has the potential to be augmented through the chimney effect. In the work of Tian et al. [26], a first step was given in this direction. A numerical study of using the chimney effect to optimize a panel-type radiator was performed and 19.22% increasement in the cooling capacity was obtained.

In this paper, the flow and heat transfer of a novel panel-type radiator under ONAN mode are numerically investigated by adding non-intrusive components. The wind deflectors were added on both lateral sides of a traditional panel-type radiator to form a chimney structure and a chimney cap was added at the top of the radiator to extend the chimney channel and further augment the chimney effect. Especially, the effects of the main geometrical parameters, including the channel numbers and chimney cap height of the chimney channel on the flow and heat transfer characteristics of panel-type radiator were firstly investigated.

2. Physical model and computational method

2.1. Physical model

The schematic diagram [27] of a 3-D panel-type radiator (PC1200-14/520) is presented in Fig. 1(a). The radiator is made of 1 mm-thick carbon steel and it consists of two 80 mm diameter (D) manifolds and 14 fins (N). These fins are equally spaced with d=45 mm, and their height (H) is 1200 mm and width (W) is 520mm. To simplify the model, the oil passage of the radiator is simplified to a rectangular channel with a thickness of 6 mm [12]. The top of the panel-type radiator is equipped with a chimney cap, whose channel number is N', and the length, width and height are $L'\times W'\times H'$, respectively. The wind deflectors are installed on both lateral sides of the radiator. The thickness of the chimney cap and wind deflectors is both 5 mm and their material is acrylic with low thermal conductivity. To simplify the calculation, half of the computational domain is used by introducing the symmetry option. According to literature [28], the natural convection air domain should contain at least 3 times of the characteristic length in the flow direction, and other directions should contain at least half of the characteristic length. This conclusion was also confirmed by Zhang et al. [29]. The computational domain and boundaries are shown in Figs. 1(b) and 1(c), where the height (H) of the

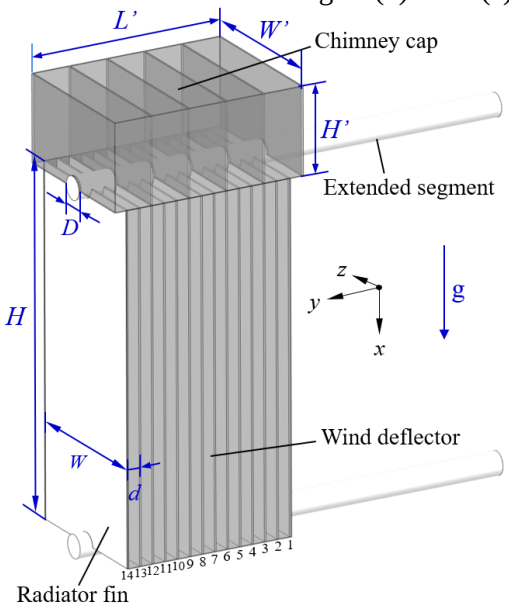

(a) Full model

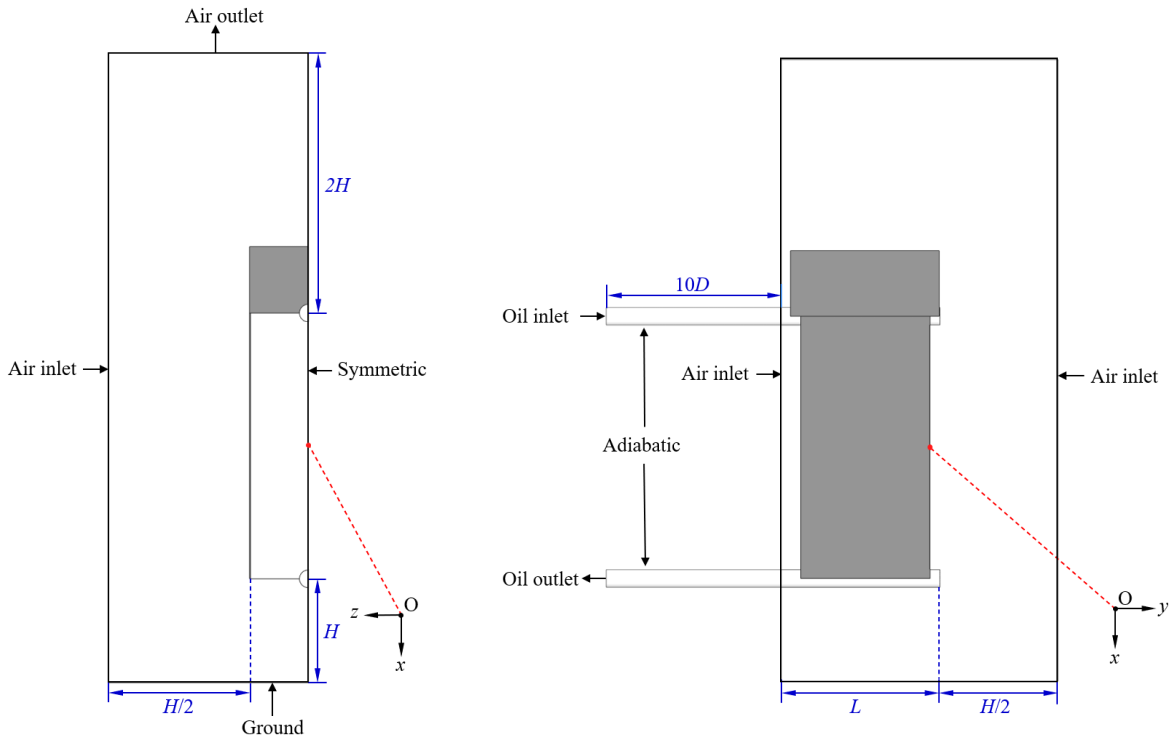

(b) Side view **(c) Back view**

Figure 1. Schematic of the physical model, computational domain and its boundary conditions for a panel-type radiator (PC1200-14/520)

radiator fin is selected as the characteristic length of the airflow. A more detailed summary of the boundary conditions is given in Tab. 1. In order to make the model closer to the real conditions, the two manifolds of the panel-type radiator are extended by 10 times of the pipe diameter, so the oil-flow inside panel-type radiator can be regarded as fully developed flow. Since this paper mainly focuses on the flow and heat transfer improvement with the chimney effect, the radiation heat transfer is not considered, which is similar to the study of literature [30].

Table 1. Boundary conditions used for the physical model

Boundary	Condition	Settings	
Oil inlet	Mass flow inlet	q_m = 0.1335 kgs^{-1}[31]	T = 343.05 K[31]
Oil outlet	Pressure outlet	p = 0 Pa	T = 298 K
Air inlet	Pressure inlet	p = 0 Pa	T = 298 K
Air outlet	Pressure outlet	p = 0 Pa	T = 298 K
Ground	Temperature	T = 303 K	\
Chimney cap	Coupled wall	\	\
Wind deflector	Coupled wall	\	\
Extended segment	Adiabatic wall	\	\
Radiator fin	Coupled wall	Shell conduction(1mm)	\

2.2. Computational method

A three-dimensional, steady-state, incompressible turbulent flow and heat transfer model was adopted to formulate natural convection heat transfer for the air in the radiator. Its governing equations can be expressed as in Eqs. (1)-(3), respectively. For turbulence flow, the shear-stress transport (SST) k-ω was used [32].

$$\frac{\partial}{\partial x_i}(\rho u_i) = 0 \tag{1}$$

$$\frac{\partial}{\partial x_i}(\rho u_i u_j) = -\frac{\partial p}{\partial x_i} + \frac{\partial}{\partial x_i}\left[\mu\left(\frac{\partial u_i}{\partial x_j} + \frac{\partial u_j}{\partial x_i} - \frac{2}{3}\delta_{ij}\right)\right] + \rho g\beta(T - T_0) - \frac{\partial}{\partial x_i}(\rho\overline{u_i' u_j'}) \tag{2}$$

$$\frac{\partial}{\partial x_i}(\rho u_i c_p T) = \frac{\partial}{\partial x_i}\left(\lambda\frac{\partial T}{\partial x_i}\right) - \frac{\partial}{\partial x_i}(\rho\overline{u_i' T'}) \tag{3}$$

where u_i and u_j are the partial velocities in different directions, m s^{-1}; i and j denote the tensor notation; p is the pressure, Pa; T is the temperature, K; x_i is the direction of coordinates, m; ρ is the density of fluid, kg m^{-3}; μ is the dynamic viscosity, kg m^{-1} s^{-1}; δ_{ij} is the Kronecker delta; β is the thermal expansion coefficient, K^{-1}; T_0 is the reference temperature of air, K; λ is the thermal conductivity, W m^{-1} K^{-1}; c_p is the specific heat at constant pressure, J kg^{-1} K^{-1}.

Kim et al. [33] pointed out that, due to the low flow rate of insulating oil inside the panel-type radiator, the oil-flow pattern can be considered as laminar flow. Therefore, the momentum and energy equations for the oil flow could be formulated as follows:

$$\frac{\partial}{\partial x_i}(\rho u_i u_j) = -\frac{\partial p}{\partial x_i} + \frac{\partial}{\partial x_i}\left[\mu\left(\frac{\partial u_i}{\partial x_j} + \frac{\partial u_j}{\partial x_i} - \frac{2}{3}\delta_{ij}\right)\right] + g(\rho - \rho_0) \tag{4}$$

$$\frac{\partial}{\partial x_i}(\rho u_i c_p T) = \frac{\partial}{\partial x_i}\left(\lambda\frac{\partial T}{\partial x_i}\right) \tag{5}$$

The heat conduction equation for the solid part of the radiator can be expressed as in Eq. (6).

$$\frac{\partial}{\partial x_i}\left(\lambda_s\frac{\partial T}{\partial x_i}\right) = 0 \tag{6}$$

Equations (1)-(6) are solved using finite volume method (FVM) implemented in Ansys Fluent. The convective terms in the momentum and energy equations are discretized with the second-order upwind scheme. A 3-D, steady-state and segregated solver was used with a COUPLED algorithm for the coupling between velocity and pressure. The convergence criterion is set to below 10^{-5}. The Boussinesq assumption was used in the air domain to characterize the effect of buoyancy forces induced by the temperature difference. The air reference temperature (T_0) was set as 298 K and the thermal expansion coefficient (β) was 0.0033 K^{-1} [13]. Other typical thermal parameters of the materials used in the simulation are shown in Tab. 2.

Table 2. Typical thermal parameters in the simulation[1, 25]

	ρ [kg m^{-3}]	λ [W m^{-1} K^{-1}]	c_p [J kg^{-1} K^{-1}]	μ [kg m^{-1} s^{-1}]
Steel	7850	88	455	\
Oil	1067.75-0.6376T	0.15217-7.16×$10^{-5}T$	821.19+3.563T	0.08467-4×$10^{-4}T$+5×$10^{-7}T^2$
Air	1.170	0.262	1007	1.86×10^{-5}
Acrylic	1180	0.2	1549	\

2.3. Grid Independence Test and Model Validations

The mesh as shown in Fig. 2(a) is the Polyhedra mesh generated by using Fluent meshing. There are 3-layer boundary layer mesh with a growth rate of 1.1 on both sides of the wall. A thin prism mesh with thickness of 0.15 mm near the wall was used for the boundary layer, which can meet

the requirements of the SST *k*-*ω* turbulence model for the wall mesh ($\overline{y^+}$=0.29) [34]. To improve simulation accuracy, a region-refined meshing technique was used. Different mesh setups were obtained by increasing the boundary layer grids and changing the local mesh dimensions. Figure 2(b) shows the variation of cooling capacity (*Q*) and outlet oil temperature of the panel-type radiator for different grids. When the number of grids reaches 2.24×10^7, further grid refinement produces only 0.66% and 0.01% differences in cooling capacity and outlet oil temperature, respectively. Therefore, it can be judged that the numerical results should be independent of the grid when its number reaches 2.24×10^7.

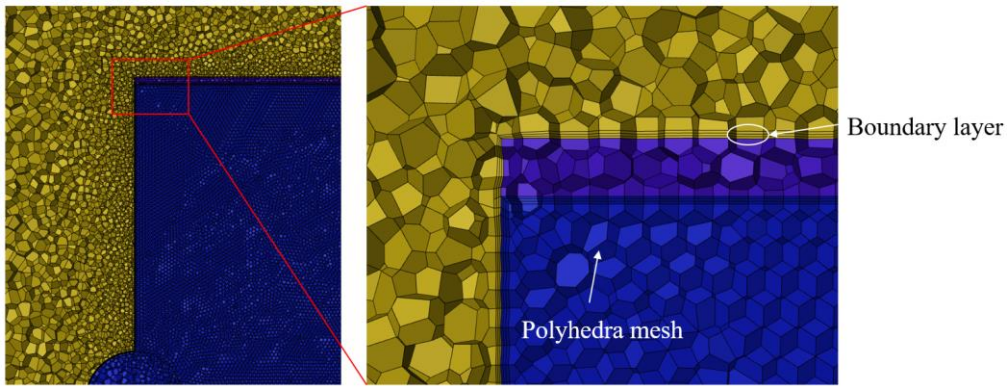

(a) Computational Mesh

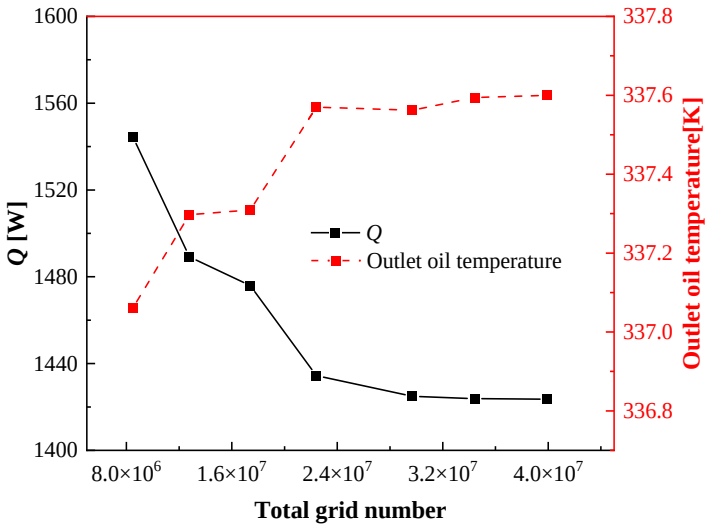

(b) Variations of cooling capacity and outlet oil temperature with different grids

Figure 2. Computational mesh and grid-independent test

Furthermore, in order to verify the numerical method, a validation of the study by Kim et al. [12] was carried out. A panel-type radiator with dimensions of 520 mm (*W*) × 2500 mm (*H*) × 30 (*N*) in ONAN mode was simulated. The model parameters are shown in Tab. 3. The inlet oil temperature and mass flow rate are 348.15 K and 44.4 L min^{-1}, respectively. The ambient temperature is 293.15 K.

Table 3. Geometrical parameters for model validation

Parameter	The diameter of two manifolds	The length of two manifolds	The diameter of the radiator fins	The distance of each fin	The thickness of fins
Value [mm]	76.2	2500	10	35	1

The overall heat transfer coefficient and cooling capacity of a panel-type radiator in literature [12] and present simulation were compared. The overall heat transfer coefficient can be expressed as:

$$\bar{h}=\frac{Q}{S(T_{\mathrm{oil,avg}}-T_{\infty})} \tag{7}$$

where S is the surface area of the traditional radiator, m^2; T_{∞} is the ambient air temperature, K; $T_{\mathrm{oil,avg}}$ is the volume-averaged oil temperature, K, which can be expressed as:

$$T_{\mathrm{oil,avg}}=\frac{1}{V_{\mathrm{oil}}}\int_{V_{\mathrm{oil}}} T_{\mathrm{oil}}\mathrm{d}V \tag{8}$$

where V_{oil} represents the oil volume, m^3.

As shown in Tab. 4, The cooling capacity of the panel-type radiator for the present simulation is 17154.9 W, and the overall heat transfer coefficient ($\bar{h}$) is 4.8 W m^{-2} K^{-1}. Compared with the numerical simulation results of Kim et al. [12], the deviation of the cooling capacity is 6%, and the deviation of the overall heat transfer coefficient is 10.34%. As compared with their experimental results [12], the deviation of cooling capacity is 12.35%.

Table 4. Model validation results

	Present simulation	Simulation results in Ref. [12]	Deviation	Experiment results in Ref. [12]	Deviation
Cool capacity [W]	17154.9	18250.0	6%	19571.9	12.35%
$\bar{h}$ [W m^{-2} K^{-1}]	4.80	5.35	10.34%	\	\

3. Results and discussion

3.1. Effect of wind deflectors and chimney cap

The temperature along the panel-type radiator gradually decreases from top to bottom and the mass flow rate of air is constant in enclosed channels. According to the principle of the chimney effect, as the air temperature rises, its density decreases, and its volume flow rate consequentially rises. Therefore, in this study, the first consideration is to enclose both lateral sides of the panel-type radiator so that the air domain between the fins can form enclosed channels with deflectors. Then, the impact of adding a chimney cap at the top of the radiator to extend the length of the chimney channel is also discussed. The specific settings of above cases are shown in Tab. 5.

Table 5. Settings for different cases

Case	Settings
1	Without wind deflectors and chimney cap
2	With wind deflectors
3	With wind deflectors and chimney cap(N' = 1, H' = 300 mm)

Figure 3 shows the temperature distributions at the center cross-section (x = 0 mm) of the panel-type radiator for the cases in Tab 5. In Fig. 3(a), it can be clearly observed that the thermal boundary layer on the surface of the radiator fins in Case 1 gradually becomes thicker along the negative direction of the z-axis, which is similar to the flat-plate flow and suggests that there exists air flowing

from both lateral sides of the panel-type radiator into the inter-channel. As shown in Fig. 3(b), when two wind deflectors are added at the *z*-axis direction of the radiator, the temperature field in the air domain changes obviously, and the thickness of the thermal boundary layer on the fin surface becomes thinner. Since the lateral sides of the radiator are enclosed and airflow can not flow into the channel from lateral sides, the thermal boundary layer becomes relatively thick on the surface of the wind deflectors. In Fig. 3(c), it can be found that the temperature field at the middle plane of the radiator (x = 0 mm) does not change obviously after additioning the chimney cap at the top of the radiator as compared with Case 2. Figures 4(a)-4(c) show the velocity and streamline distributions of air between the 7th and 8th radiator fins (y = -295.5 mm). In Fig. 4(a), the air side-suction phenomenon is quite obvious at both lateral sides of the panel-type radiator without wind deflectors, which is consistent with that presented in Fig. 3(a). This phenomenon is due to the fact that the ambient temperature around the radiator is lower than the air temperature in the channel between the fins. As air flows from the bottom and lateral sides of the radiator at the same time under the thermal pressure difference, the airflow at different directions will influence with each other. As shown in Fig. 4(b), when wind deflectors are added, the side suction of air is completely blocked, and the airflow velocity between radiator fins is obviously increased. Meanwhile, it can also be observed that the air flow distribution between radiator fins becomes more uniform, and the air and insulating oil inside the radiator will form a counter-current flow with higher heat transfer efficiency. In addition, it also shows that part of the air at the lateral side of the radiator flows into the bottom of the radiator under the thermal pressure difference and forms a small recirculation zone at the inlet of the channel. As shown in Fig. 4(c), when a chimney cap is added at the top of the radiator, the area of the high-speed air zone at the top of the radiator increases, and the air at this zone is less affected by the horizontal airflow.

For the chimney effect, the airflow is accelerated due to the thermal pressure difference. Figs. 4(d)-4(f) show the pressure distributions of air between radiator fins for different cases. For the conventional panel-type radiator in Fig. 4(d), the air pressure between radiator fins is almost equal to the atmospheric pressure, and a local negative pressure zone is observed only near the top of the upper manifold, which is similar to the flow around a circular cylinder. When the wind deflectors are added, as shown in Fig. 4(e), a large negative pressure zone is formed in the air domain between the radiator fins, and the air pressure in the lower half of the radiator is lower than that in the upper half of the radiator. Since the radiator is enclosed, the air at the bottom of the radiator can produce greater driving force, which will drive more cold air flow into the bottom of the radiator. Finally, as shown in Fig. 4(f),

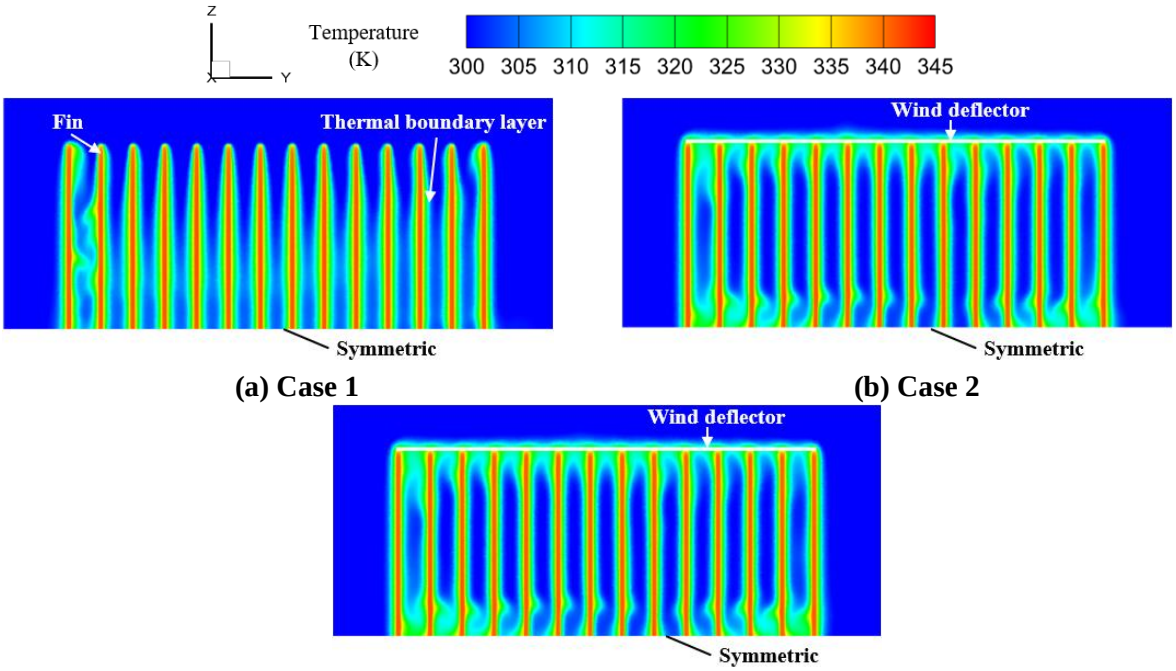

Figure 3. Temperature distributions at the *yz* plane (*x* = 0 mm) in the panel-type radiator for different cases

by adding a top chimney cap at the top of the radiator, the negative pressure zone of the air in the channel is extended, the average pressure between the radiator fins is further reduced, and the chimney effect is enhanced.

According to the study of Bacharoudis et al. [35], the static pressure reduction at the chimney inlet can be expressed as in Eq. (9):

$$p_{\mathrm{dra}} = p_{\mathrm{in}} - p_{\infty} = -\frac{1}{2}\rho V^2 \tag{9}$$

where p_{dra} is the static pressure reduction at the chimney inlet, Pa; p_{in} is air static pressure at the inlet; p_{∞} is the static pressure of the environment, Pa; and V is the average velocity of air, m s^{-1}.

The static pressure reduction at the chimney inlet, also known as the chimney draft pressure, depends on the chimney height and density difference between the ambient air and air at the chimney inlet (without taking into account chimney wall friction) [23].

$$p_{\mathrm{dra}} = (\rho_{\mathrm{in}} - \rho_{\infty})g(H + H') \tag{10}$$

where, ρ_{∞} is the density of the ambient air, m^3, and ρ_{in} is the density of the inlet air at the bottom of the chimney, m^3. Equations (9) and (10) are obtained based on Bernoulli's equation, which can be used to predict the chimney draft pressure and reveal the reason for airflow acceleration in the chimney channel. It is noticed from Figs. 4(b) and 4(c) that, the direction of airflow entering the bottom of the radiator is perpendicular to the height direction of the chimney, which will generate oblique airflow acceleration and form vortices at the inlet of the channels. This will further reduce the local static

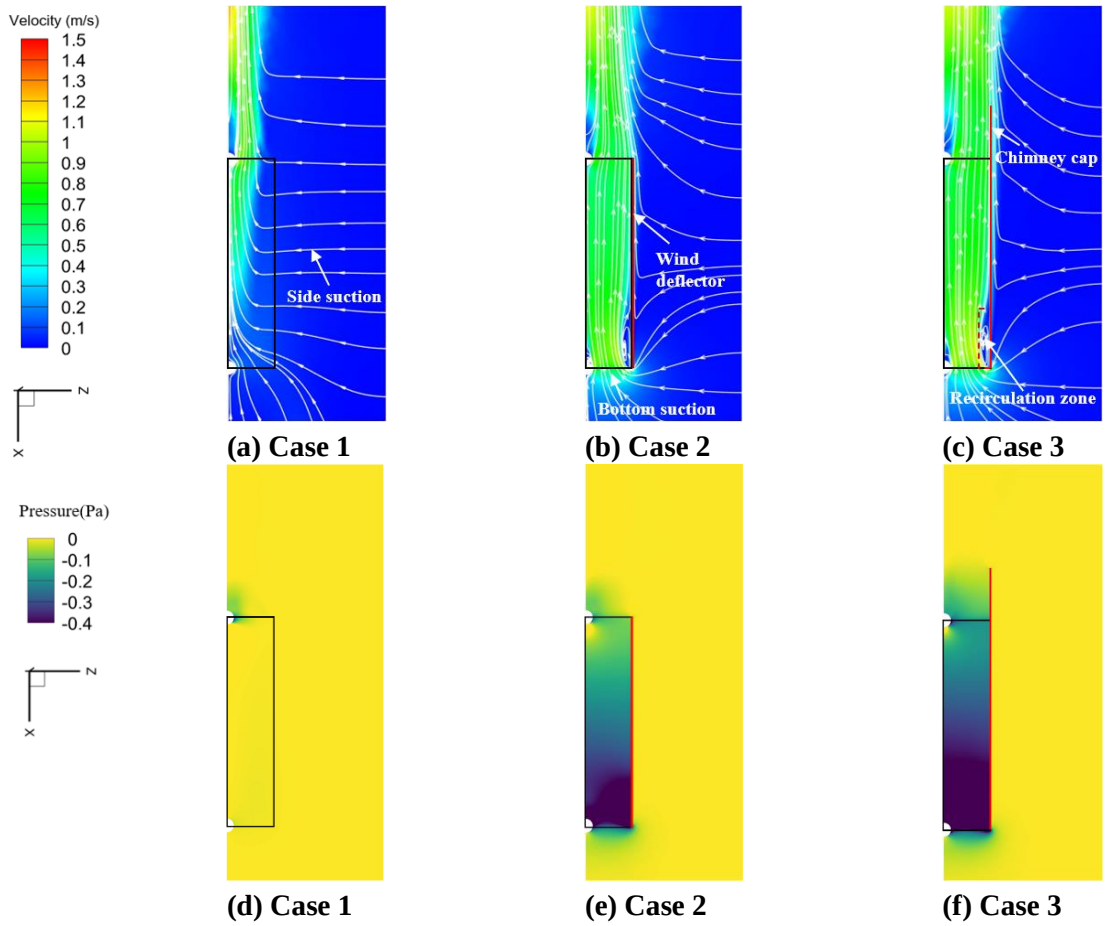

Figure 4. Velocity and pressure distributions at *xz* plane (*y* = -295.5 mm) in the panel-type radiator for different cases

pressure at the corner of the chimney inlet and form airflow recirculation zones. According to the study of literature [23], such sharp edges can increase the pressure difference, which is favorable for increasing air flow rate and enhancing heat transfer.

Figure 5(a) shows the variations of total air flow rate, bottom air flow rate and side air flow rate between radiator fins for different cases. It shows that, the total air flow rate in a conventional panel-type radiator (Case 1) is less than that in other two cases, while the side air flow rate in this case accounts for 72.8% of the total air flow rate. In case 1, the side air flow and bottom air flow interfere with each other, which will reduce the total air flow rate and heat dissipation as well. When the wind deflectors are added at the lateral sides of the radiator (Case 2), the side air suction is completely blocked, and it is observed that, the total air flow rate is increased by 11.35% and the cooling capacity is improved by 12.57%. When the top chimney cap is added at the top of the radiator (Case 3), the chimney effect is further enhanced, the total air flow rate is increased by 18.29% and the cooling capacity is improved by 15.74%. Figure 5(b) shows the distributions of insulating oil mass flow rate in different radiator fins for different cases. For the conventional radiator (Case 1), the flow distribution tends to be large on both sides and small in the middle, which is consistent with the findings in the literature [3]. This phenomenon is due to the fact that end fins of the radiator are directly exposed to ambient air with better heat dissipation performance, which makes the oil temperature in the fins lower and produces stronger thermosiphon, thus increasing the oil flow rate [29]. When the oil flows from the upper manifold, the pressure loss increases gradually as the flow path grows, thus the fins at the

two ends of the radiator have different oil mass flow rates. With addition of the wind deflectors (Case 2), the oil mass flow rate distribution in the radiator is more uniform. In addition, a sudden drop in the oil flow rate in the secondary end fins of the radiator (the 2nd and 13th fins) is observed. This is because the chimney effect created by the inter-fin channels has an aggregation effect on the air with the addition of wind deflectors. This will result in slower airflow, thicker flow boundary layer, and weaker heat transfer in the channels at both ends of the radiator. Similar phenomenon can also be observed in Fig. 3(b). Due to the presented air flow characteristics in the end channels, the cooling capacity and oil mass flow rate of the two fins at both ends of the radiator decrease. Finally, in Case 3, the addition of the top chimney cap resulted in a further improvement in the uniformity of oil flow distribution in the radiator, but its overall distribution trend was similar to the Case 2.

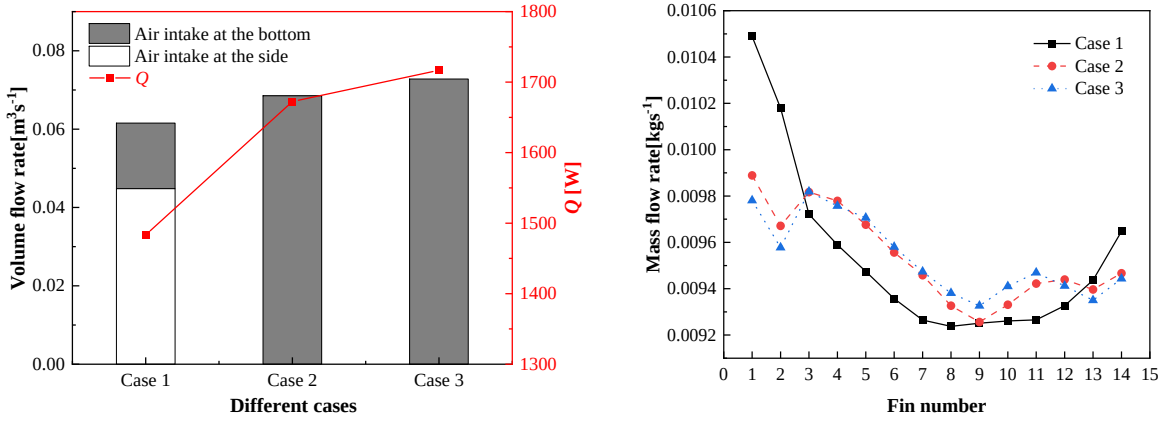

(a) Variations of Air Volume Flow Rate and Heat Dissipation of Radiator under Different Operating Conditions

(b) Insulating oil mass flow rate distributions in different radiator fins

Figure 5. Performance comparison for panel-type radiator under different cases

3.2. Effect of chimney cap structural parameters

In this section, the effect of top chimney cap height (H'=300 mm, 500 mm, 700 mm) and the number of chimney cap channels (N'=1, 3, 5, 15) on the cooling performance of the novel panel-type radiator is analyzed. Fig. 6 and Fig. 7 show the velocity and pressure distributions of the panel-type radiator at the *xy* plane (z = 0 mm) for different chimney cap configurations, respectively. Fig. 8 shows the performance variation of the panel-type radiator for different chimney cap configuration parameters.

From Figs. 6(a)-6(l), it shows that, the area of the high-speed flow zone at the top of the radiator becomes larger and more uniform as N' increases, which indicates the air velocity and flow uniformity enhances gradually. In addition, it is found that obvious recirculation flow is formed at the medium channels of the chimney cap. From Figs. 7(a)-7(l), it shows that, this recirculation flow phenomenon is caused by the air as it sweeps over the upper manifold and a negative pressure zone is produced at the top of the upper manifold. However, since the bottom of the lateral channels of the chimney cap is connected to the ambient environment, the negative pressure gradient is relatively small, and the recirculation flow is not formed at the bottom of lateral channels of the chimney cap.

From Fig. 8(b), it shows that, as H' increases from 300 mm to 500 mm, the cooling capacity of the radiator is enhanced by 2.54%, 3.34%, 3.37% and 2.63% at N'=1, 3, 5 and 15, respectively, and the $\bar{h}$ is enhanced by 3.02%, 4.00%, 4.01% and 3.11%, respectively. As H' further increases to 700 mm, the cooling capacity of the radiator is increased by 2.94%, 6.18%, 7.26% and 4.75%, respectively, as compared with those at H'=300 mm, and the $\bar{h}$ is enhanced by 3.48%, 7.56%, 8.35% and 5.65%, respectively. Therefore, increasing the height of the chimney cap can enhance the cooling performance of the panel-type radiator in this study. As can be seen in Fig. 7, when the H' increases, the area of the negative air pressure zone between the radiator fins increases gradually, and the negative pressure zone inside the chimney cap extends upward. Therefore, the airflow path formed by the panel-type radiator together with the wind deflectors and top chimney cap can create a larger pressure difference between the air inside and the atmosphere, namely the chimney draft pressure (P_{dra}). From Eqs. (9) and (10), it can be supposed that the air volume flow rate in the flow channel become larger as chimney channel extends, which can also be confirmed by Fig. 8(a). Furthermore, In Fig. 8, it is noticed that when N'=1, increasing H' from 500 mm to 700 mm, changes in the volume flow rate of air and cooling capacity of the radiator are relatively small. Figs. 6(e) and 6(i) show the velocity distributions under above two conditions, respectively. In Fig. 6(e), it can be observed that the airflow at the top of the radiator tilts toward the positive direction of y-axis. When H' increases to 700 mm, as shown in Fig. 6(i), the airflow tilts much more. Correspondingly in Figs. 7(e) and 7(i), the above phenomenon is reflected in an asymmetric distribution of negative air pressure zones at the top of the radiator, which results in a larger negative air pressure zone in the left half of the chimney cap. That is because, when N'=1, as H' increases, the total heat dissipated from the 8th to 14th radiator fins is larger than that from 1st to 7th radiator fins. This means, the air exchanges more heat with the second half of the radiator, which causes the airflow tilt to the right at the top of the radiator. As the airflow tilts more, an obvious cold inflow [36] is observed in Fig. 6(i). This phenomenon is created by the density difference between the hot air in the chimney channel and cold ambient air at the top of the radiator, which typically occurs near the unheated wall of the asymmetrically heated vertical channels [37]. Cold inflow can hinder the mainstream air flow and decrease the air flow rate, which is not conducive to the heat transfer enhancement. In addition, from Fig. 8(b), it is found that, when $N' \leq 5$, the cooling capacity of the panel-type radiator increases gradually as N' increases. As shown in Figs. 6(a)-6(c), 6(e)-6(g), 6(i)-6(k), it is noticed that, the area of the high-velocity airflow region at the top of the radiator increases as N' increases, and the uniformity of the airflow is also improved. Correspondingly in Figs. 7(a)-(c), 7(e)-7(g), 7(i)-7(k), the area of the negative air pressure zone between radiator fins increases as N' increases, and the chimney draft pressure also increases. Therefore, from Fig. 8(a), it can be found that the volume flow rate of air at the top of the radiator increases with the increase of N', which can enhance the convective heat transfer between radiator fins. When N' is further increased to 15, it is shown in Figs. 6(d), 6(h) and 6(l) that, the airflow uniformity is further enhanced. While from Fig. 8(a), it can be found that when H' is relatively small (H'=300 mm), increasing N' to 15 can increase air flow rate and enhance heat dissipation of the radiator. However, when H' increases to 500

mm or 700 mm, increasing H' to 15 will decrease the flow rate of air and reduce the cooling capacity of the radiator instead. This is because, as the chimney cap height increases, the uniformity of the airflow increases, but the frictional resistance created by the channel wall also increases.

The purpose of heat transfer performance enhancement of the panel-type radiator is to reduce its outlet oil temperature, which in turn reduces the operating temperature of the transformer. Therefore, the outlet oil temperature of the panel-type radiator for different cases are also compared in Fig. 8(c). It is obvious that, the tendency of outlet oil temperature for different case are opposite to that of the cooling capacity. As cooling capacity increases, the outlet oil temperature decreases and vice versa. When H'=700 mm and N'=5, the outlet oil temperature reaches a minimum value of 335.95 K.

In this study, the best cooling capability of the panel-type radiator is obtained when the chimney cap height is H'=700 mm and the number of chimney cap channels is N'=5. As compared with the traditional panel-type radiator, the cooling capacity and overall heat transfer coefficient of the novel radiator under this condition can be increased by 26.54% and 28.21%, respectively, and the temperature difference between the inlet and outlet insulating oil is 7.1 ℃.

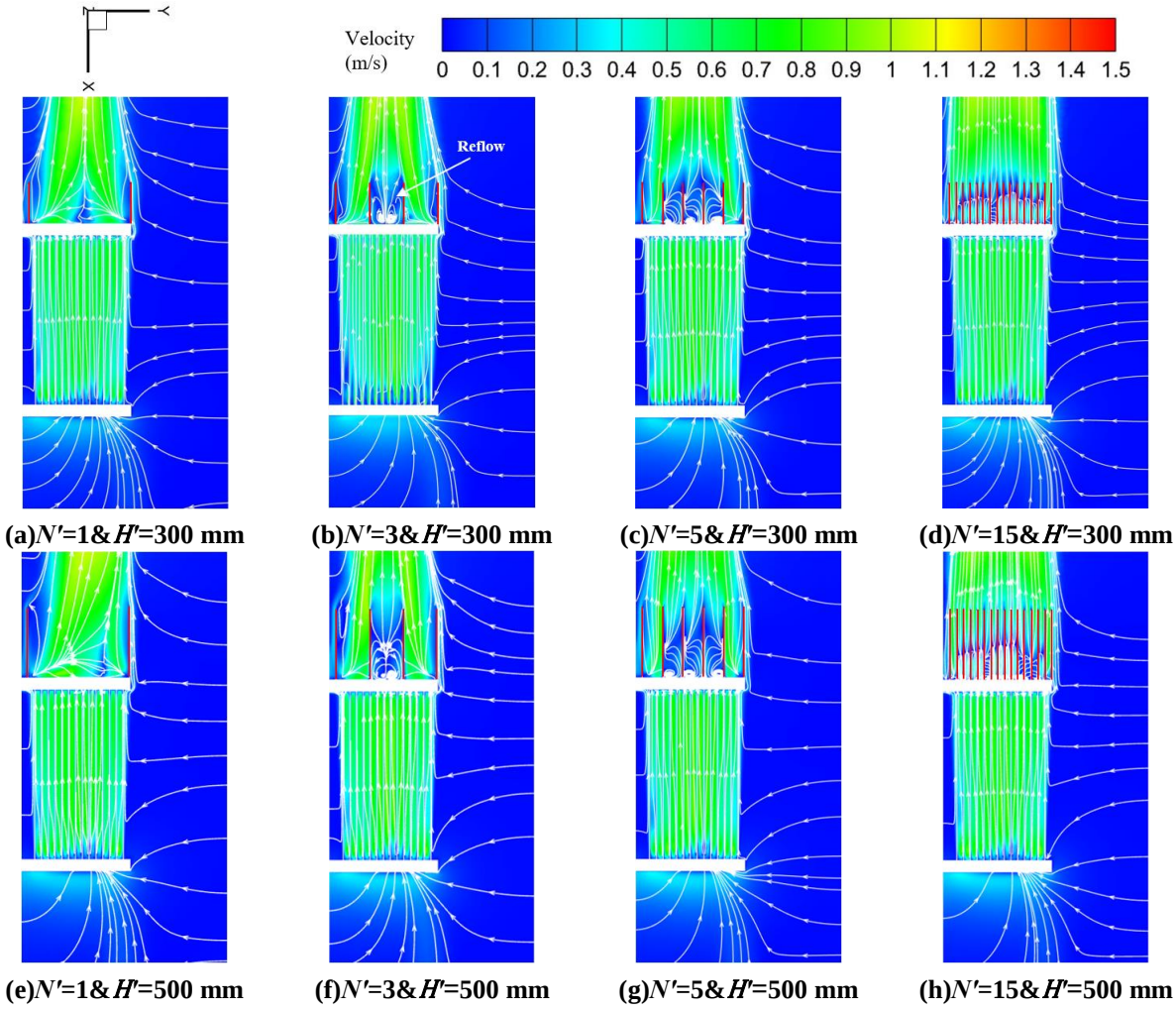

(a)N'=1&H'=300 mm **(b)N'=3&H'=300 mm** **(c)N'=5&H'=300 mm** **(d)N'=15&H'=300 mm**

(e)N'=1&H'=500 mm **(f)N'=3&H'=500 mm** **(g)N'=5&H'=500 mm** **(h)N'=15&H'=500 mm**

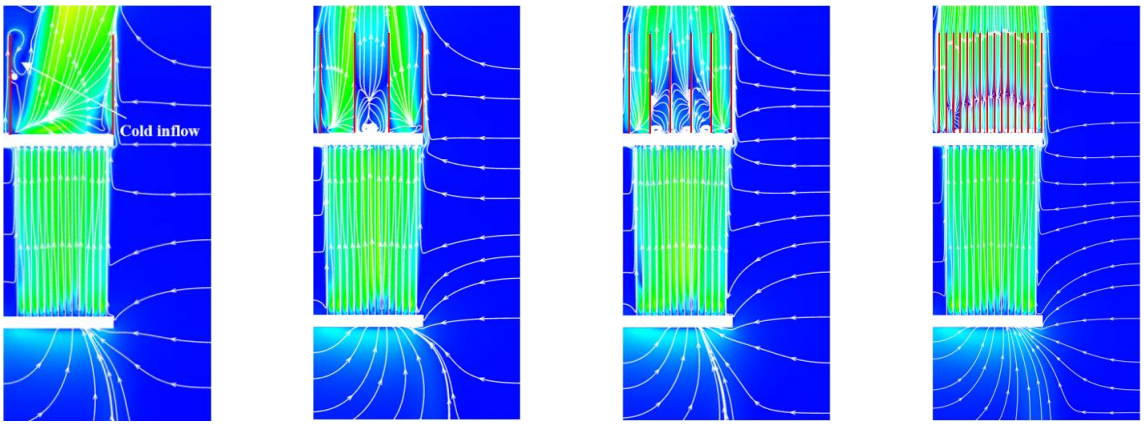

(i)N'=1&H'=700 mm (j)N'=3&H'=700 mm (k)N'=5&H'=700 mm (l)N'=15&H'=700 mm

Figure 6. Velocity distributions at *xy* plane (*z* = 0 mm) in the panel-type radiator with different chimney cap configurations

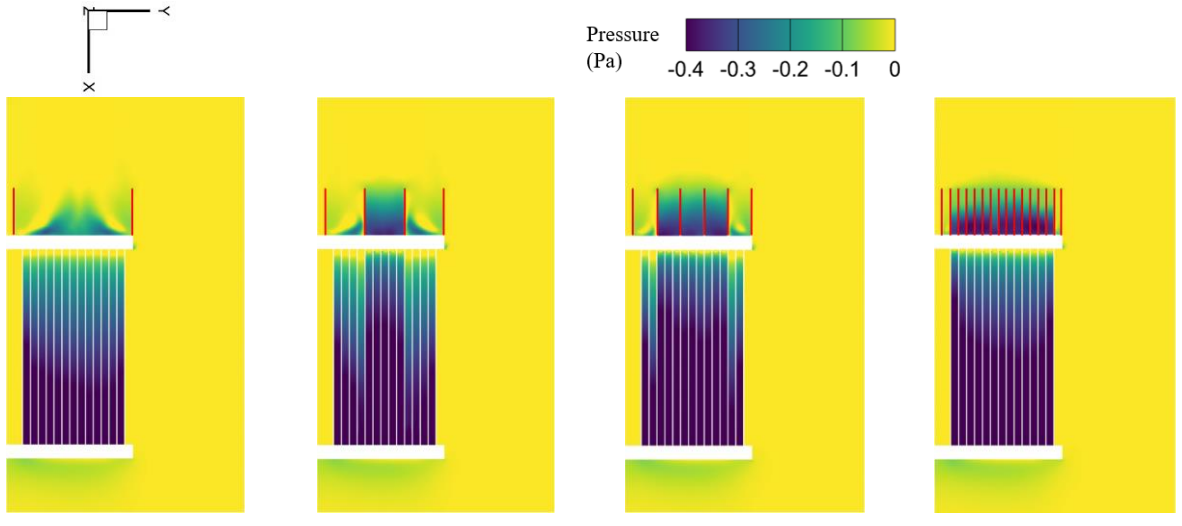

(a)N'=1&H'=300 mm (b)N'=3&H'=300 mm (c)N'=5&H'=300 mm (d)N'=15&H'=300 mm

(e)N'=1&H'=500 mm (f)N'=3&H'=500 mm (g)N'=5&H'=500 mm (h)N'=15&H'=500 mm

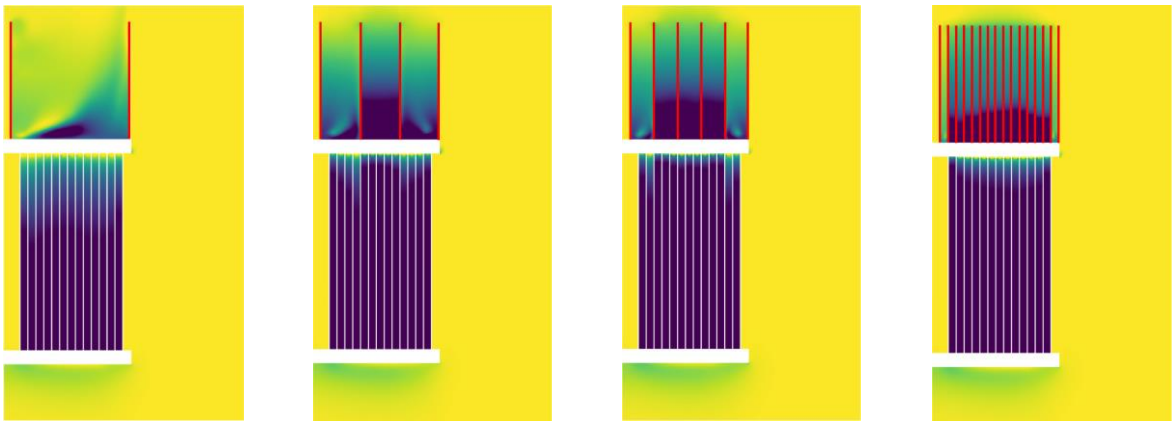

(i)N'=1&H'=700 mm (j)N'=3&H'=700 mm (k)N'=5&H'=700 mm (l)N'=15&H'=700 mm

Figure 7. Pressure distributions at *xy* plane (*z* = 0 mm) in the panel-type radiator with different chimney cap configurations

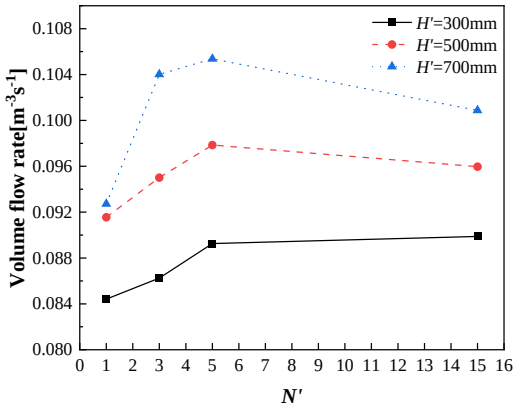

(a) Variations of air volume flow rate at the top of the radiator

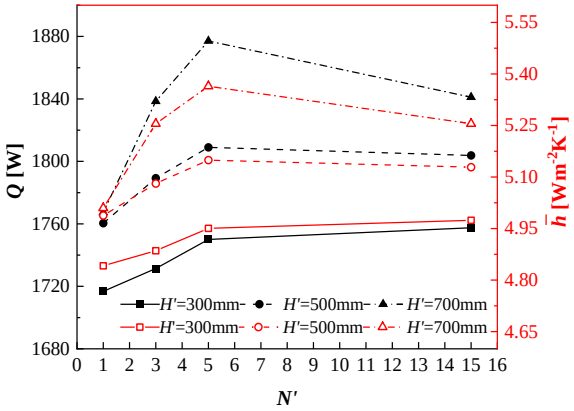

(b) Variations of cooling capacity and overall heat transfer coefficient

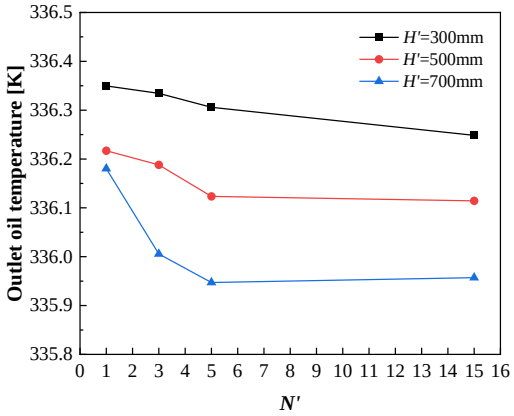

(c) Variations of outlet oil temperature

Figure 8. Performance variations of panel-type radiators with different chimney cap structural parameters

4. Conclusion

In this paper, the panel-type radiator for the transformer under ONAN mode was improved based on the chimney effect, and its flow and heat transfer characteristics were numerically

investigated. Firstly, the effect of adding wind deflectors on both lateral sides and a chimney cap on the top of the radiator on its thermal performance was investigated. Secondly, the effect of the chimney cap structural parameters (height, and number of channels) on the thermal performance of the panel-type radiator was analyzed. The main conclusions are as follows:

Firstly, since the air can be sucked from the top and both lateral sides of traditional panel-type radiator simultaneously, the air inflow at different directions will influence with each other, which will result in thicker thermal boundary layer near the wall of radiator fins, and the cooling performance is poor. The wind deflectors can form enclosed air channels with the radiator fins. Influenced by the chimney effect, a large negative air pressure area is created in the channel and an upward suction effect is generated, which will accelerate the airflow. As the side air flow is completely blocked, the air and the insulting oil in the radiator can form a counter-current heat transfer, which ultimately improves the cooling capacity of the radiator by 12.75%. In addition, adding a chimney cap to the top of the radiator can further extend the length of the chimney channel, and the radiator's cooling capacity is increased by 15.74%.

Secondly, increasing the height of the chimney cap (H') will increase the area of the negative air pressure zone between radiator fins and increase the chimney draft pressure. Meanwhile, increasing the number of chimney cap channels (N') can enhance the uniformity of the airflow, but both of above methods will produce larger frictional resistance. When N' and H' are relatively large, further increases in N' and H' will reduce air flow rate in the radiator and reduce its thermal performance. In this study, the best thermal performance of the panel-type radiator is obtained at H'=700 mm and N'=5. As compared with the traditional radiator, the cooling capacity and overall heat transfer coefficient of the novel radiator are increased by 26.54% and 28.21%, respectively, and the temperature difference between the inlet and outlet insulating oil is 7.1 ℃.

Acknowledgment

This work was supported by the S&T project of State Grid Shanghai Municipal Electrical Power Company under grant number of 52094022000Y.

Nomenclature

c_p	specific heat at constant pressure [J kg^{-1} K^{-1}]	δ_{ij}	kronecker delta
D	manifolds diameter [mm]	λ	thermal conductivity [W m^{-1} K^{-1}]
d	radiator fin spacing [mm]	μ	dynamic viscosity [kg m^{-1} s^{-1}]
g	gravity acceleration [m s^{-2}]	ρ	density [kg m^{-3}]
H	radiator fin height [mm]	***Subscripts***	
H'	chimney cap height [mm]	dra	draft
$\bar{h}$	overall heat transfer coefficient [W m^{-2} K^{-1}]	i,j	different dimensions of tensor
L'	chimney cap length [mm]	in	inlet
N	radiator fin number	m	mass
N'	number of chimney cap channels	oil	insulating oil
p	pressure [Pa]	oil,avg	volume-averaged oil
Q	cooling capacity [W]	s	solid

q_m	mass flow rate of transformer oil [kg s^{-1}]	∞	ambient
S	surface area of traditional radiator [m^2]	***Abbreviations***	
T	temperature [K]	AF	Air Forced cooling
u	velocity component [m s^{-1}]	AN	Air Natural cooling
V	average air velocity [m s^{-1}]	FVM	Finite Volume Method
W	radiator fin width [mm]	OD	Oil Directed cooling
W'	chimney cap width [mm]	OF	Oil Forced cooling
x, y, z	cartesian coordinates [mm]	ON	Oil Natural cooling
y^+	dimensionless wall distance	PC	Removeable panel-type radiator
Greek symbols		SST	Shear-Stress Transport
β	thermal expansion coefficient [K^{-1}]	TEG	Thermoelectric Generators

References

[1] Kim, M. G., et al., Prediction and Evaluation of the Cooling Performance of Radiators Used in Oil-Filled Power Transformer Applications with Non-Direct and Direct-Oil-Forced Flow, *Experimental Thermal and Fluid Science*, 44(2013), pp. 392-397, doi: org/10.1016/j.expthermflusci.2012.07.011.

[2] Kassi, K. S., Fofana, I., Studying Power Transformers Cooling Effectiveness from Computational Fluid Dynamics Approach, *Proceedings*, 2016 IEEE Electrical Insulation Conference (EIC), Montréal, Canada, 2016, pp. 13-16.

[3] Chandak, V., *et al.*, Numerical Investigation to Study Effect of Radiation on Thermal Performance of Radiator for Onan Cooling Configuration of Transformer, *IOP Conference Series Materials Science and Engineering*, 88(2015), pp. 012033, doi: 10.1088/1757-899X/88/1/012033.

[4] Xu, D. P., *et al.*, Analysis of Winding Temperature Field under Dynamic Variable Load of Oil-Immersed Transformer, *Thermal Science*, 25 (2021), 4B, pp. 3009-3019, doi: org/10.2298/TSCI211015041L.

[5] Cha, C. H., *et al.*, Investigation of the Thermal Head Effect in a Power Transformer, Transmission & Distribution Conference & Exposition: Asia and Pacific, Seoul, Korea (South), 2009, pp. 641-712, doi: 10.1109/TD-ASIA.2009.5356811.

[6] Tălu, S. D., Tălu, M. D., Dimensional Optimization of Frontal Radiators of Cooling System for Power Transformer 630 kVA 20/0.4 kV in Terms of Maximum Heat Transfer, *University Politehnica of Bucharest Scientific Bulletin, Series C*, 72 (2010), 4, pp. 249-260.

[7] Kim, Y. J., *et al.*, Numerical Study on the Effect of the Shape of the Heat Transfer Plate on the Thermal Performance of the Radiator(in Korean), *Journal of Computational Fluids Engineering*, 20 (2015), 1, pp. 65-76, doi: org/10.6112/kscfe.2015.20.1.065.

[8] Min, C., *et al.*, Numerical Investigation of Natural Convection Heat Transfer for Panel Type Radiator Mounted with Longitudinal Vortex Generators, *Proceedings*, 2011 International Conference on Materials for Renewable Energy & Environment, Shanghai, China, 2011, pp. 1267-1270, doi: 0.1109/ICMREE.2011.5930567.

[9] Fdhila, R. B., *et al.*, Thermal Modeling of Power Transformer Radiators Using a Porous Medium Based CFD Approach, *Proceedings*, 2nd International Conference on Computational Methods for Thermal Problems (THERMACOMP 2011), Dalian, China, 2011, pp. 1-4.

[10] Paramane, S. B., *et al.*, CFD Study on Thermal Performance of Radiators in a Power Transformer: Effect of Blowing Direction and Offset of Fans, *IEEE Transactions on Power Delivery*, 29 (2014), 6, pp. 2596-2604, doi: 10.1109/TPWRD.2014.2347292.

[11] Paramane, S. B., Flow and Temperature Visualization over Radiators of Transformer using Experimental and Advanced CFD Simulations, *Proceedings*, International conference on

Advances in Thermal Systems, Materials and Design Engineering (ATSMDE2017), Mumbai, India, 2017, doi.org/10.2139/ssrn.3102052.

[12] Kim, Y. J., *et al*., A Numerical Study of the Effect of a Hybrid Cooling System on the Cooling Performance of a Large Power Transformer, *Applied Thermal Engineering*, 136(2018), pp. 275-286, doi: org/10.1016/j.applthermaleng.2018.03.019.

[13] Garelli, L., *et al*., Heat Transfer Enhancement in Panel Type Radiators Using Delta-wing Vortex Generators, *International Journal of Thermal Sciences*, 137(2019), pp. 64-74, doi: org/10.1016/j.ijthermalsci.2018.10.037.

[14] Li, Y. G., *et al*., Analysis of External Heat Dissipation Enhancement of Oil-immersed Transformer Based on Falling Film Measure, *Thermal Science*, 26(2022), 6(Part A), pp. 4519-4533, doi: org/10.2298/TSCI211015041L.

[15] Ding, Y. D., *et al*., Experimental and Numerical Investigation on Natural Convection Heat Transfer Characteristics of Vertical 3-D Externally Finned Tubes, *Energy*, 239(2022), pp. 122050, doi: org/10.1016/j.energy.2021.122050.

[16] Rodriguez, G. R., *et al.*, Numerical and Experimental Thermo-fluid Dynamic Analysis of a Power Transformer Working in ONAN Mode, *Applied Thermal Engineering*, 112(2017), pp. 1271-1280, doi: org/10.1016/j.applthermaleng.2016.08.171.

[17] Abbas, A., Wang, C.C., Augmentation of Natural Convection Heat Sink Via Using Displacement Design, *International Journal of Heat and Mass Transfer*, 154(2020), pp. 119757, doi: org/10.1016/j.ijheatmasstransfer.2020.119757.

[18] Asadi, S., *et al.*, The Effect of Solar Chimney Layout on Ventilation Rate in Buildings, *Energy and Buildings*, 123(2016), pp. 71-78, doi: org/10.1016/j.enbuild.2016.04.047.

[19] Khidhir, D. K., Atrooshi, S.A., Investigation of Thermal Concentration Effect in a Modified Solar Chimney, *Solar Energy*, 206(2020), pp. 799-815, doi: org/10.1016/j.solener.2020.06.011.

[20] Haaland, S. E., Sparrow, E.M., Solutions for the Channel Plume and the Parallel-walled Chimney, *Numerical Heat Transfer*, 6(1983), pp. 155-172, doi: org/10.1080/01495728308963080.

[21] Auletta, A., *et al*., Heat Transfer Enhancement by the Chimney Effect in a Vertical Isoflux Channel, *International Journal of Heat and Mass Transfer*, 44(2001), 22, pp. 4345-4357, doi: 10.1016/s0017-9310(01)00064-3.

[22] Moon, J. Y., *et al*., Influence of Chimney Width on the Natural Convection Cooling of a Vertical Finned Plate, *Nuclear Engineering and Design*, 293(2015), pp. 503-509, doi: org/10.1016/j.nucengdes.2015.08.012.

[23] Abbas, A., *et al*., Investigation of Performance Augmentation for Natural Convective Heatsink with the Help of Chimney, *Applied Thermal Engineering*, 178(2020), pp. 115586. doi: org/10.1016/j.applthermaleng.2020.115586.

[24] Schwurack, R., *et al*., Performance Enhancement of a Thermoelectric System with Improved Natural Convection Cooling by Utilizing the Chimney Effect, *Energy Conversion and Management*, 237(2021), pp. 114118, doi: org/10.1016/j.enconman.2021.114118.

[25] Fulpagare, Y., *et al*., Experimental and Numerical Investigation of Natural Convection for a Fully Closed Cabinet Subject to Chimneys, *International Journal of Thermal Sciences*, 183(2023), pp. 107889. doi: org/10.1016/j.ijthermalsci.2022.107889.

[26] Tian, Y. H., *et al.*, Numerical Study on Hydrodynamic and Heat Transfer Performances for Panel-Type Radiator of Transformer Using the Chimney Effect, Chemical Engineering Transactions, 103(2023), pp. 163-168, doi: org/10.3303/CET23103028.

[27] Nitulescu, T., Talu, S., *Applications of Descriptive Geometry and Computer Aided Design in Engineering Graphics*, Risoprint Publishing house, Cluj-Napoca, Romania, 2001, ISBN: 973-656-102-X.

[28] Wang, Y. K., *Basic Course of ANSYS Icepak Electronic Heat Dissipation (2nd Edition) (in Chinese)*, National Defense Industry Press, Beijing, CHN, 2018, ISBN: 9787121350207.

[29] Zhang, K., *et al*., Experimental and Numerical Investigation of Natural Convection Heat Transfer of W-type Fin Arrays, *International Journal of Heat and Mass Transfer*, 152(2020), pp. 119315, doi: org/10.1016/j.ijheatmasstransfer.2020.119315.

[30] Kim, N. H., Cho, J.P., Air-side Performance of Louver-finned Flat Aluminum Heat Exchangers at a Low Velocity Region, *Heat and Mass Transfer*, 44(2007), pp. 1127-1139. doi: org/10.1007/s00231-007-0346-4.

[31] Paramane, S.B., *et al.*, A Coupled Internal-external Flow and Conjugate Heat Transfer Simulations and Experiments on Radiators of a Transformer, *Applied Thermal Engineering*, 103(2016), pp. 961-970, doi: org/10.1016/j.applthermaleng.2016.04.164.

[32] Menter, F. R., Two-equation Eddy-viscosity Turbulence Models for Engineering Applications, *AIAA Journal*, 1994(8), 32, pp. 1598-1605, doi: org/10.2514/3.12149.

[33] Kim, Y. J., Ha, M. Y., A Study on the Performance of Different Radiator Cooling Systems in a Large-scale Electric Power Transformer, *Journal of Mechanical Science and Technology*, 31(2007), 7, pp. 3317-3328, doi: 10.1007/s00231-007-0346-4.

[34] Jia, H. N., *et al.*, Numerical Investigation of Heat Transfer Enhancement with Dimpled Particles in Structured Packed Beds, *Heat Transfer Research*, 53(2022), 17, pp. 19-40, doi: 10.5487/res.18792.

[35] Bacharoudis, E., *et al.*, Study of the Natural Convection Phenomena Inside a Wall Solar Chimney with One Wall Adiabatic and One Wall under a Heat Flux, *Applied Thermal Engineering*, 27(2007), 13, pp. 2266-2275, doi: 10.1016/j.applthermaleng.2007.01.021.

[36] Sparrow, E. M., *et al.*, Observed Flow Reversals and Measured-predicted Nusselt Numbers for Natural Convection, *Journal of Heat Transfer*, 166(1984), pp. 325-332, doi: org/10.1115/1.3246676.

[37] Fisher, T. S., Torrance, K. E., Experiments on Chimney-enhanced Free Convection, *Journal of Heat Transfer*, 121(1999), 3, pp. 603-609, doi: org/10.1115/1.2826022.

Received: 26.09.2023.

Revised: 07.01.2024.
Accepted: 08.01.2024